High-resolution Free-breathing late gadolinium enhancement Cardiovascular magnetic resonance to diagnose myocardial injuries following COVID-19 infection

Aurelien Bustin, Soumaya Sridi, Pierre Gravinay, Benoit Legghe, Philippe Gosse, Alexandre Ouattara, Hadrien Roze, Pierre Coste, Edouard Gerbaud, Arnaud Desclaux, et al.

European Journal of Radiology 144 (2021) 109960

Contents lists available at ScienceDirect

European Journal of Radiology

journal homepage: www.elsevier.com/locate/ejrad

High-resolution Free-breathing late gadolinium enhancement Cardiovascular magnetic resonance to diagnose myocardial injuries following COVID-19 infection

Aurélien Bustin [a,b,c,*,1], Soumaya Sridi [a,1], Pierre Gravinay [d], Benoit Legghe [a], Philippe Gosse [d], Alexandre Ouattara [e], Hadrien Rozé [e], Pierre Coste [f], Edouard Gerbaud [f], Arnaud Desclaux [g], Alexandre Boyer [h], Renaud Prevel [h], Didier Gruson [h], Fabrice Bonnet [i], Nahema Issa [j], Michel Montaudon [a], François Laurent [a], Matthias Stuber [b,c,k], Fabrice Camou [j], Hubert Cochet [a,b]

[a] Department of Cardiovascular Imaging, Groupe Hospitalier Sud, CHU Bordeaux, Pessac, France
[b] IHU LIRYC, Electrophysiology and Heart Modeling Institute, Université de Bordeaux – INSERM U1045, Avenue du Haut Lévêque, Pessac, France
[c] Department of Diagnostic and Interventional Radiology, Lausanne University Hospital and University of Lausanne, Lausanne, Switzerland
[d] Cardiac Intensive Care Unit, Hôpital St André, CHU Bordeaux, Bordeaux, France
[e] Department of Anaesthesia and Critical Care, Groupe Hospitalier Sud, CHU Bordeaux, Pessac, France
[f] Cardiac Intensive Care Unit, Groupe Hospitalier Sud, CHU de Bordeaux, Pessac, France
[g] Infectious disease Unit, Hôpital Pellegrin, CHU Bordeaux, Bordeaux, France
[h] Medical Intensive Care Unit, Hôpital Pellegrin, CHU Bordeaux, Bordeaux, France
[i] Infectious Disease Unit, Hôpital St André, CHU Bordeaux, Bordeaux, France
[j] Intensive Care Unit, Hôpital St André, CHU Bordeaux, Bordeaux, France
[k] CIBM Center for Biomedical Imaging, Lausanne, Switzerland

ARTICLE INFO

Keywords:
Cardiac Magnetic Resonance Imaging
High-resolution
Late Gadolinium Enhancement
COVID-19

ABSTRACT

Purpose: High-resolution free-breathing late gadolinium enhancement (HR-LGE) was shown valuable for the diagnosis of acute coronary syndromes with non-obstructed coronary arteries. The method may be useful to detect COVID-related myocardial injuries but is hampered by prolonged acquisition times. We aimed to introduce an accelerated HR-LGE technique for the diagnosis of COVID-related myocardial injuries.

Method: An undersampled navigator-gated HR-LGE (acquired resolution of 1.25 mm^3) sequence combined with advanced patch-based low-rank reconstruction was developed and validated in a phantom and in 23 patients with structural heart disease (test cohort; 15 men; 55 ± 16 years). Twenty patients with laboratory-confirmed COVID-19 infection associated with troponin rise (COVID cohort; 15 men; 46 ± 24 years) prospectively underwent cardiovascular magnetic resonance (CMR) with the proposed sequence in our center. Image sharpness, quality, signal intensity differences and diagnostic value of free-breathing HR-LGE were compared against conventional breath-held low-resolution LGE (LR-LGE, voxel size 1.8x1.4x6mm).

Results: Structures sharpness in the phantom showed no differences with the fully sampled image up to an undersampling factor of x3.8 ($P > 0.5$). In patients ($N = 43$), this acceleration allowed for acquisition times of 7min21s ± 1min12s at 1.25 mm^3 resolution. Compared with LR-LGE, HR-LGE showed higher image quality ($P = 0.03$) and comparable signal intensity differences ($P > 0.5$). In patients with structural heart disease, all LGE-positive segments on LR-LGE were also detected on HR-LGE (80/391) with 21 additional enhanced segments visible only on HR-LGE (101/391, $P < 0.001$). In 4 patients with COVID-19 history, HR-LGE was definitely positive while LR-LGE was either definitely negative (1 microinfarction and 1 myocarditis) or inconclusive (2 myocarditis).

Abbreviations: HR-LGE, High-resolution late gadolinium enhancement; CMR, Cardiovascular magnetic resonance; LR-LGE, Low-resolution late gadolinium enhancement; LGE, Late gadolinium enhancement; MINOCA, Myocardial infarction with non-obstructed coronary arteries; 3D, Three-dimensional; PCR, Polymerase chain reaction; ECG, Electrocardiogram; LV, Left ventricle; TI, Inversion time; RV, Right ventricular; EF, Ejection fraction; TTE, Transthoracic echocardiography; ROI, Regions-of-interest; BMI, Body mass index.

* Corresponding author at: IHU LIRYC, Electrophysiology and Heart Modeling Institute Université de Bordeaux, Avenue du Haut Lévêque, 33604 Pessac, France.
E-mail address: aurelien.bustin@ihu-liryc.fr (A. Bustin).

[1] Aurélien Bustin and Soumaya Sridi contributed equally to the study and are co-first authors.

https://doi.org/10.1016/j.ejrad.2021.109960
Received 31 May 2021; Received in revised form 30 August 2021; Accepted 15 September 2021
Available online 20 September 2021

Conclusions: Undersampled free-breathing isotropic HR-LGE can detect additional areas of late enhancement as compared to conventional breath-held LR-LGE. In patients with history of COVID-19 infection associated with troponin rise, the method allows for detailed characterization of myocardial injuries in acceptable scan times and without the need for repeated breath holds.

1. Introduction

One major concern related to the recent COVID-19 pandemic lies in the impact of the infection on the myocardium [1]. Several large series have reported high rates of myocardial injuries in hospitalized patients (20–36%), with cardiac involvement being a major factor of adverse outcome [2–4]. Multiple mechanisms can lead to cardiac damage, including type 1 myocardial infarction, type 2 myocardial infarction, stress cardiomyopathy, microvascular ischemia, and myocarditis [5]. Cardiovascular magnetic resonance (CMR) plays a pivotal role in identifying the underlying mechanism in myocardial infarction with non-obstructed coronary arteries (MINOCA) [6], and was thus proposed to detect and characterize COVID-related myocardial injuries. A recent study reported than 49% of patients with history of COVID-19 and troponin rise had positive late gadolinium enhancement (LGE) on CMR [7,8]. The burden that these scars may weigh on the infected population over the long term remains uncertain. Considering the prognostic role of LGE in structural heart diseases and acute coronary syndromes, LGE CMR may play an important role to stratify the risk of future adverse outcomes after COVID-19 infection.

All prior CMR studies in COVID patients have employed conventional LGE techniques acquired during breath holds. While providing good contrast between the injured and healthy myocardial tissue, these techniques have inherently low spatial resolution, which can affect their ability to resolve small myocardial defects (14). In addition, conventional LGE techniques require repeated breath-holds, which can be difficult to perform in COVID-19 patients. High resolution three-dimensional (3D) LGE methods acquired during free-breathing were shown valuable to improve the sensitivity of CMR in the context of MINOCA and to enhance the diagnostic value in atrial fibrosis assessment as well as for the detection of small myocardial scars in ischemic and non-ischemic cardiomyopathies [9–11]. These methods may be useful to detect subtle COVID-related myocardial injuries, particularly in patients with persistent dyspnoea, but remain restrained by quite prolonged acquisition times (~8–12 min for anisotropic resolution [9] and ~ 16 min at 1.4 mm^3 isotropic resolution [12,13]). The increasing need for CMR in the context of COVID imposes an optimization of clinical workflows, and accelerated techniques are thus critically needed.

The aim of the present study was to introduce an accelerated free-breathing high-resolution 3D LGE technique to optimize the detection and characterization of COVID-related myocardial injuries.

2. Material and methods

2.1. Study design and patients

The study design consisted of 3 steps. Firstly, the accelerated high resolution free breathing 3D LGE sequence was tested and optimized in a resolution phantom. Secondly, it was validated in a series of patients with known structural heart disease (test group; N = 23) to document its incremental value over a conventional LGE method in detecting myocardial injuries. These patients were imaged between June 2020 and September 2020 and were not consecutive as the inclusion depended on the clinical workflow. The inclusion criteria were an indication for CMR as part of standard care, and a history of structural heart disease of ischemic or non-ischemic origin. Exclusion criteria were any contra-indications to CMR. Thirdly, the method was applied in patients with history of COVID-19 infection associated with troponin rise (COVID group; N = 20), to assess the spectrum of COVID-related myocardial injuries at high spatial resolution. These were consecutive patients prospectively included from May 2020 to November 2020. Inclusion criteria were laboratory confirmed COVID-19 infection associated with troponin rise. Patients requiring mechanical ventilation and those with persistent positive polymerase chain reaction (PCR) testing were not considered for inclusion. The study was approved by an ethics committee, and all patients provided informed consent.

2.2. Whole-heart high-resolution diaphragmatic navigated undersampled 3D LGE

HR-LGE was performed using a free-breathing, three-dimensional, inversion-recovery-prepared, electrocardiogram (ECG)-gated, respiration-navigated gradient-echo pulse sequence (Fig. 1). A SPIR (spectral presaturation with inversion recovery) fat saturation pulse was used to minimize fat-related artefacts. The sequence was accelerated using a 3D variable density Cartesian trajectory [14,15] that samples the k_y-k_z phase-encoding plane following approximate spiral interleaves on the Cartesian grid with variable density along each spiral arm (i.e., the k-space center being fully sampled with exponentially increased undersampling towards the periphery). This pseudo-random sampling scheme results in noise-like artefacts in the image domain, which are desired from a reconstruction and compressed-sensing point of view [16]. A spectrally selective crossed-pair navigator preceded each spiral-like interleave to dynamically track the respiratory motion of the heart. An acceptance window of ± 3 mm was placed in end-expiration.

Imaging parameters are provided in Table 1. As opposed to our previous HR-LGE sequence [9], where 3D data was acquired with mild undersampling factors (GRAPPA x2) and anisotropic resolution (1.25 × 1.25 × 2.5 mm), our proposed isotropic (1.25 mm^3) HR-LGE sequence exploits higher undersampling factors (3.8-fold) to achieve clinically feasible (sub-10 min) acquisition times. With such undersampling factor, the image reconstruction pipeline needs to be adapted to compensate for the increased noise due to the ill-posed nature of the reconstruction problem. A patch-based low-rank reconstruction was used to recover high quality LGE images [14]. This reconstruction framework assumes that the 3D HR-LGE data contains a rich amount of redundancy on a local (i.e., within a small patch) and non-local (i.e., between similar patches within a spatial neighbourhood) scales. This redundancy information can be exploited through patch-based matrix representation and singular value truncation to regularize the overall reconstruction problem. The different steps of the reconstruction algorithm are detailed in [14,17]. To assess the full clinical performance of the proposed HR-LGE sequence, the patch-based reconstruction was written in C++ and integrated into the scanner reconstruction software (Image Calculation Environment, Siemens Healthcare, Erlangen, Germany).

2.3. Phantom study

A multi-purpose resolution phantom (Siemens Healthcare, Erlangen, Germany) was imaged with the proposed HR-LGE framework to evaluate the impact of undersampling on image sharpness and resolution. The phantom contains 55 holes with varying diameters in a range of [1.1; 11.5 mm] (Fig. 2). Data was acquired assuming 100% respiratory scan efficiency at a simulated heart rate of 70 beat-per-minute. Different undersampling factors were tested ([1, 2.5, 3.8, 5.2]). The relevant imaging parameters are reported in Table 1. The nominal field-of-view

was chosen to be 23 cm^3 for a spatial resolution of 1.25 mm^3. Sharpness was measured for each undersampled image at holes' edges as $\frac{1}{d}$ (in mm^{-1}) with d being the distance transitioning from 80% to 20% of the intensity profile (given by the minimum and maximum intensities of the profile). Sharpness values were averaged over different positions on the phantom.

2.4. Clinical CMR studies

CMR was performed on a 1.5 T clinical scanner (MAGNETOM Aera, Siemens Healthcare, Erlangen, Germany) with a dedicated 32-channel spine coil and an 18-channel body coil. The CMR protocol (Supplementary Fig. 1) comprised Cine SSFP imaging in 2-chamber, 3-chamber, 4-chamber views, and in a stack of contiguous short axis slices encompassing the ventricles. T2, T1 and ECV mapping were also performed in a stack of contiguous short axis slices covering the whole left ventricle (LV).

LR-LGE (reconstructed spatial resolution of 1.5 × 1.5 × 4.0 mm) imaging was performed 10 min after the administration of 0.2 mmol/kg gadoteric acid using a breath-held and inversion recovery-prepared turbo FLASH sequence in 3 stacks of contiguous slices encompassing the ventricles in short-axis, 2-chamber, 3-chamber and 4-chamber orientations. HR-LGE imaging was initiated 15–20 min post contrast at higher isotropic spatial resolution (reconstructed voxel size 0.6 mm^3), as detailed above. For HR-LGE imaging, an additional inversion time (TI) scout scan was performed after conventional LR-LGE imaging. Acquisition times and scan efficiency (i.e., percentage of data within the respiratory gating window) for HR-LGE imaging were recorded.

2.5. CMR analysis

LV and right ventricular (RV) volumes, ejection fraction (EF) and wall motion abnormalities were analysed by experienced observers (S.S. and H.C.) using a dedicated software (CVI42, Circle Cardiovascular Imaging, Calgary, Canada). The distribution of LGE was categorized as subendocardial, subepicardial, and/or midwall. LGE was considered transmural if involving the entire myocardial thickness on at least one location. The criteria to diagnose myocardial infarction were the presence of subendocardial or transmural LGE [18]. The criteria to diagnose myocarditis were the presence of definite midwall and/or subepicardial LGE in the absence of subendocardial LGE [19]. Arrhythmogenic right ventricular cardiomyopathy was diagnosed according to the Task Force Criteria [20]. The criteria to diagnose takotsubo cardiomyopathy were either a wall motion abnormality involving the entire apical or basal levels in the absence of myocardial LGE, or a similar wall motion abnormality documented on acute transthoracic echocardiography (TTE) in a patient with normal wall motion and negative LGE on CMR [18].

CMR results were interpreted in combination with the clinical history, and after reviewing the results from acute ECG, TTE and biological tests. CMR was categorized as conclusive when patients fulfilled the criteria for a definite diagnosis, and as non-conclusive otherwise.

Table 1
Acquisition parameters for conventional breath-hold low-resolution LGE (LR-LGE) and proposed free-breathing high-resolution LGE (HR-LGE).

	LR-LGE	HR-LGE
Repetition time, ms	3.9	5.2
Echo time, ms	1.7	2.5
Flip angle, degrees	10	19
Field of view, mm	360 × 290 × 101	360 × 360 × 120
Acquired resolution, mm	2.0 × 1.5 × 7.4	1.25 × 1.25 × 1.25
Reconstructed resolution, mm	1.5 × 1.5 × 4.0	0.63 × 0.63 × 0.63
Number of slices, range	11–16	96–160
Phase oversampling, %	15	20
Slice oversampling, %	0	16.7
Asymmetric echo	Yes	Yes
Acquisition window, ms	236	156
Average number of k-space lines per heartbeat	60	30
Inversion time, ms	210–300	270–350
Trajectory & Acceleration	Cartesian GRAPPA x2	Cartesian variable density x3.8
Trigger pulse, RR interval	1	1
Bandwidth, Hz/pixel	360	255
Breath-hold	Yes	No

2.6. LR-LGE versus HR-LGE analysis

LGE images were analysed by 2 readers in consensus (S.S. and A.B., two and seven years' experience in CMR, respectively), with LR-LGE and HR-LGE being reviewed separately 2 months apart, in order to ensure independent analysis of the 2 datasets. Images were reviewed on a clinical PACS-system (Carestream Health, Rochester, New York, USA), where image magnification and windowing could be optimized. Conventional LR-LGE images were reviewed in the four acquired orientations. Owing to its isotropic resolution, the HR-LGE volume could be reviewed in multiplanar reformations of any desired orientation, depending on the LGE pattern and distribution.

The overall quality of all LGE images acquired in the test and COVID-19 cohorts was graded using a four-point ordinal system (1: poor quality with large artefacts, 2: fair quality with moderate artefacts, 3: good quality with small artifacts, 4: excellent quality with no artifacts). For scores lower than 4, impaired image quality was classified as a) incomplete myocardial nulling due to sub-optimal TI, b) motion artefacts, c) noise artefacts, or d) folding artefacts. For each dataset, the presence of LGE was assessed using a three-point ordinal scale (0: definitely absent, 1: definitely present, 2: inconclusive) in each of the 17-segment of the American Heart Association model [21]. Therefore, a total of 1462 myocardial segments were analysed in patients.

Regions-of-interest (ROI) placed in the hyperenhancement area, the

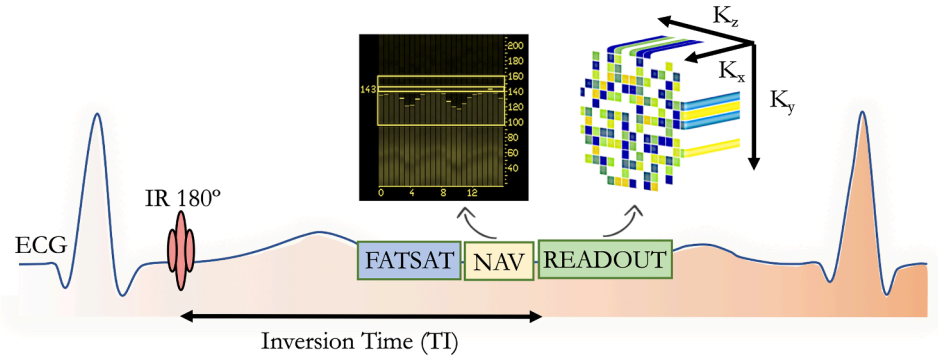

Fig. 1. Schematic overview of investigated free-breathing motion-corrected three-dimensional (3D) whole-heart high-resolution myocardial LGE framework (HR-LGE). A non-selective inversion recovery (IR) pulse is applied immediately after electrocardiogram (ECG) R wave. Image acquisition is gated to account for the diaphragmatic respiratory displacement of the heart. A variable-density Cartesian undersampling is used to achieve clinically feasible scanning times (undersampling factor of x3.8). The HR-LGE volume is reconstructed with an undersampled patch-based low-rank reconstruction exploiting local patch similarities in the 3D volume. Abbreviations: FAT SAT = fat saturation, k_x = readout, k_y = phase encoding, k_z = slice encoding, TI = inversion time.

remote myocardium, the blood pool and in a background region were extracted for each patient. Injured areas were defined as regions with LGE (based on the two standard deviations segmentation method [22]), while remote areas were defined as regions with no LGE. Mean signal intensity differences and signal ratios were determined by subtracting (respectively dividing) the signal-to-noise ratios (i.e., mean signal level divided by the noise level) of two corresponding tissues.

2.7. Statistical analysis

Results are presented using conventional descriptive statistics. The Shapiro-Wilk test was used to assess for normality. Continuous data are expressed as mean ±standard deviation when following a normal distribution, and as median [interquartile range Q1-Q3] otherwise. Categorical data are expressed as fraction (percentage). Image quality scores of the LR-LGE and HR-LGE datasets were compared using Mann-Whitney U tests. Differences in the detection of LGE segments between the two sequences were tested using the McNemar test. The influence of body mass index (BMI) and heart rate on image quality, presence of artefacts and presence of LGE was assessed using regression analysis. Continuous variables were compared using independent-sample parametric (unpaired Student's *t*-test). Statistical tests were 2-tailed. A P value < 0.05 was considered to indicate statistical significance. Statistical analysis was performed using IBM SPSS Statistics (version 26.0).

3. Results

3.1. Phantom study

The total scan times, assuming 100% respiratory gating efficiency, were 15 min 10 sec (x1), 6 min 4 sec (x2.5), 4 min 3 sec (x3.8) and 3 min 3 sec (x5.2) with 1.25 mm^3 isotropic resolution. Reconstructed images using the proposed patch-based reconstruction are shown in Fig. 2 in comparison with the reference fully sampled image. Aliasing artifacts can be observed for high undersampling factors (x5) whereas high image quality can be appreciated for undersampling factors up to x3.8, with clear depiction of the phantom structures. Structure sharpness was preserved with the proposed approach (Supplementary Fig. 2) showing no statistical differences with the reference fully sampled image ($P > 0.5$), as opposed to the standard zero-filling reconstruction ($P < 0.01$).

3.2. Image characteristics in patients

The mean acquisition time for HR-LGE was 7 min 21 sec ± 1 min 12 sec [min: 3 min 58 sec, max: 9 min 0 sec], with a mean scan efficiency of 42 ± 10 %. The typical image reconstruction time was 1 min.

The overall image quality was significantly higher on HR-LGE compared with LR-LGE (3.65 ± 0.59 vs. 3.09 ± 0.85, $P = 0.03$). It was graded as excellent (score 4) in 26/41 (63 %) in HR-LGE and 17/41 (41%) in LR-LGE. Reasons for lower image quality were residual motion artefacts (17 vs. 4 patients), sub-optimal TI (7 vs. 6 patients), folding (7 vs. 1 patients), missing slices (3 vs. 0 patients) and residual noise (0 vs. 5 patients) for LR-LGE and HR-LGE, respectively. Nondiagnostic image quality (score 1) was not found in either dataset. On both LR- and HR-LGE, heart rate and BMI did not significantly relate to the image quality, the presence of artefacts, or the presence of LGE (Supplementary Fig. 3).

In terms of contrast, mean signal intensity differences between scar and blood pool and between scar and remote myocardium did not significantly differ between LR and HR-LGE images ($P = 0.51$ and $P = 0.88$, respectively). Corresponding signal ratios for LR-LGE relative to HR-LGE were 1.13 for scar/blood pool, 1.01 for scar/remote myocardium, and 1.61 for remote myocardium/blood.

3.3. CMR findings in the test cohort

Baseline characteristics of the test cohort (N = 23; 15 males; mean age 55 ± 16 years) are shown in Table 2. The final diagnosis was ischemic heart disease in 8 (35%) and non-ischemic heart disease in 15 (65%), including 8 (35%) myocarditis, 3 (13%) hypertrophic cardiomyopathy, 3 (13%) dilated cardiomyopathy, and 1 (4%) arrhythmogenic cardiomyopathy with LV involvement. A total of 391 segments were analysed in both datasets (LR-LGE and HR-LGE). Myocardial LGE was found in 23/23 patients (100%) among which 4 (17%) showed transmural patterns, 5 (22%) sub-endocardial, 13 (57%) mid-wall and 1 (4%) sub-epicardial. All enhanced segments that were visible on LR-LGE were also detected on HR-LGE (80/391, 20%) with 21 additional enhanced segments visible only on HR-LGE (101/391, 26%, $P < 0.001$).

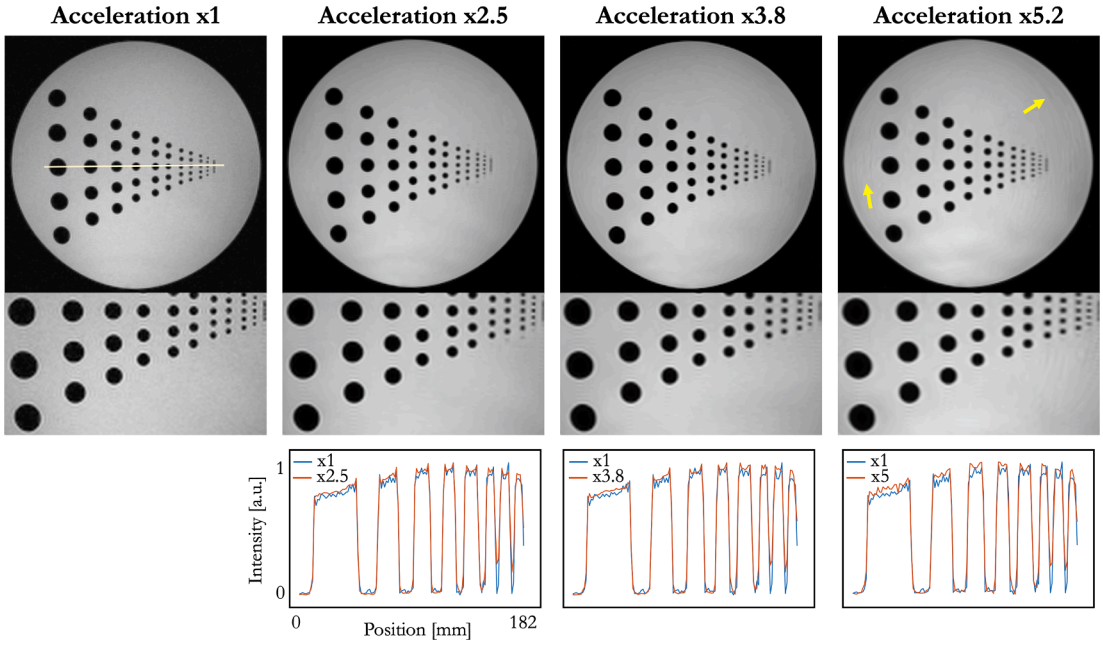

Fig. 2. Patch-based low-rank reconstructions of the resolution phantom for different undersampling factors. Reconstructed images exhibit sharp edges with faithful preservation of small details for undersampling factors up to x3.8 (as shown on the cross-section profiles).

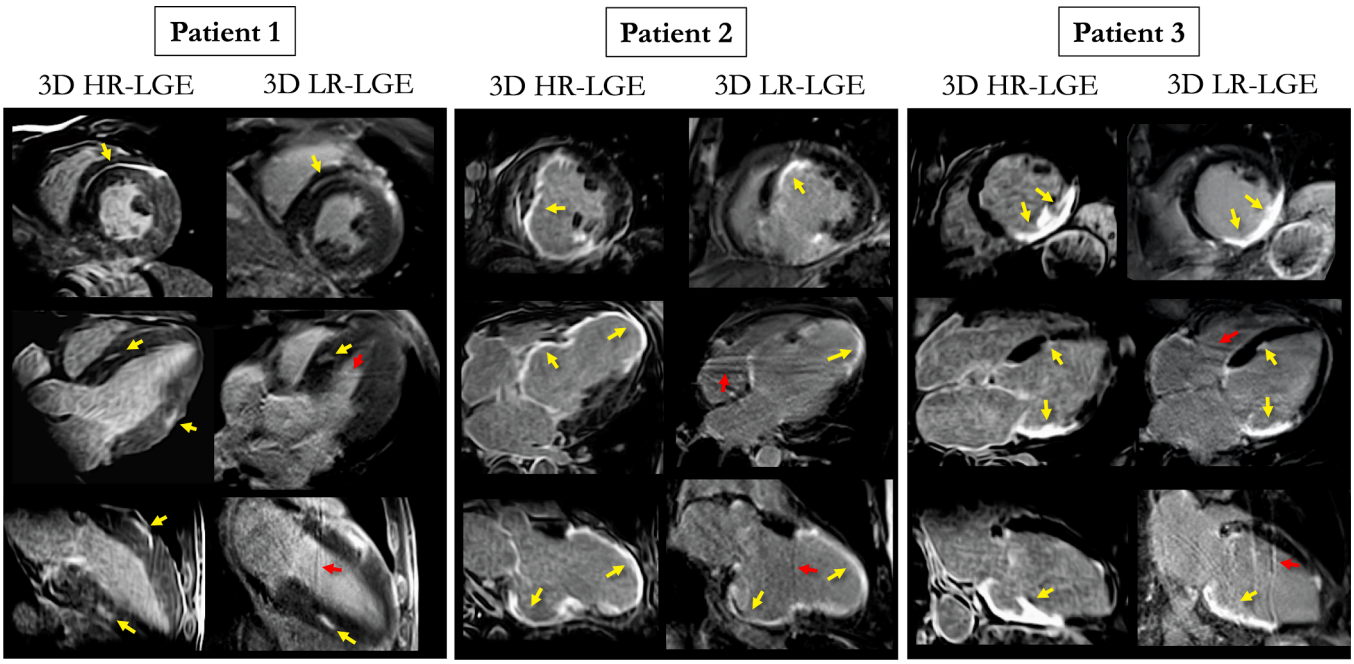

Fig. 3. Comparisons of reformatted free-breathing 3D HR-LGE and breath-held 3D LR-LGE in three patients (test cohort) with ischemic and non-ischemic LGE patterns. Yellow arrows indicate LGE, red arrows indicate artifacts on LR-LGE. *Patient 1*: 33-year-old male patient with hypertrophic cardiomyopathy associated with sub-epicardial and midwall LGE. *Patient 2*: 56-year-old male patient with ischemic cardiomyopathy showing transmural LGE in the right coronary artery and mid-left anterior descending artery territories. *Patient 3*: 75-year-old male patient presenting with severe hypokinesia and transmural myocardial infarction in the right coronary artery territory.

Table 2
Baseline characteristics of the test cohort (N = 23).

Patient characteristics	
Male gender, N (%)	15 (65)
Age, years	55 ± 16
Mean heart rate, beats/min	62 ± 9
Mean body mass index, kg/m^2	25 ± 4
CMR diagnosis	
Ischemic cardiomyopathy, N (%)	8 (35)
Non-ischemic cardiomyopathies, N (%)	15 (65)
Dilated cardiomyopathy, N (%)	3 (13)
Myocarditis, N (%)	8 (35)
Hypertrophic cardiomyopathy, N (%)	3 (13)
Arrhythmogenic right ventricular cardiomyopathy, N (%)	1 (4)
Negative CMR, N (%)	0 (0)
Cardiac function	
LVEF, %, mean ± SD	48.2 ± 16.9
Reduced LVEF, N (%)	13 (57)
LV EDV / BSA, mL/m^2, mean ± SD	109.4 ± 34.6
LV ESV / BSA, mL/m^2, mean ± SD	58.2 ± 31.5

Note: Data are expressed as mean ± standard deviation unless otherwise specified. Abbreviations: LVEF, left ventricular ejection fraction; EDV, end-diastolic volume; BSA, body surface area; ESV end-systolic volume; LGE late gadolinium enhancement.

In 3 patients, LGE was categorized as definitely absent on LR-LGE while HR-LGE showed definite mid-wall LGE. In these 3 patients, myocardial LGE was localized in the basal anteroseptal segment, the medial inferoseptal segment and the basal inferolateral and medial inferolateral segments. In 3 other patients, LGE was categorized as inconclusive on LR-LGE, while HR-LGE showed definite LGE (1 mid-wall and 2 transmural patterns). In these 3 patients, myocardial LGE was localized in the basal inferolateral and anteroseptal segments, apical lateral segment, and basal inferolateral, medial inferolateral and apical lateral segments. The benefit of 3D whole-heart isotropic resolution can be appreciated in Fig. 3. The spectrum of myocardial injuries found in the test cohort is illustrated in Fig. 4.

3.4. Characteristics of the COVID-19 cohort

The characteristics of the studied population (N = 20; 15 males; mean age 46 ± 24 years) in the acute phase of COVID-19 are shown in Table 3. Twenty patients were studied, including 2 with history of healed myocardial infarction and 18 with no history of cardiac disease. All patients had been hospitalized, including 11 in an intensive care unit, with 5 requiring mechanical ventilation. COVID-19 diagnosis was based on PCR tests in 16 and serology in 4. The median troponin peak was 305 [Q1:83 - Q3:1134] ng/L. The acute clinical presentation included chest pain in only 7/20 patients. TTE was negative in 11/20. All patients showed either negative or non-specific findings on 12-lead ECG. CMR was performed 54 [32–64] days after the onset of symptoms. At the time of the CMR study, 8/20 patients were asymptomatic, while other patients showed a variety of persistent clinical symptoms.

3.5. CMR findings in the COVID-19 cohort

Cine imaging showed wall motion abnormalities in 4/20, LV dilatation in 3/20, LVEF impairment in 4/20, and LV thrombus in 1/20 (confirmed on LGE imaging). Edema was found on T2 imaging in 10/20 patients. In 2 patients, HR-LGE imaging could not be completed due to claustrophobia. In these, a definite diagnosis could still be retained based on LR-LGE only (1 takotsubo cardiomyopathy and 1 acute myocarditis).

CMR results are listed in Table 4. Myocardial LGE was found on HR-LGE in 12/18 patients (67%), including 1 (6%) transmural, 3 (17%) subendocardial, 4 (22%) mid-wall and 4 (22%) sub-epicardial. All segments with positive LGE on LR-LGE images were also positive on HR-LGE (40/306, 13%) with 8 additional enhanced segments visible only on HR-LGE (48/306, 16%, $P < 0.01$). In 2 (11%) patients, LGE was definitely absent on LR-LGE while HR-LGE showed definite LGE (one microinfarct and one sub-epicardial LGE). In 2 (11%) other patients, LGE analysis was inconclusive on LR-LGE, whereas HR-LGE showed definite LGE (1 midwall and 1 subepicardial, Supplementary Fig. 4).

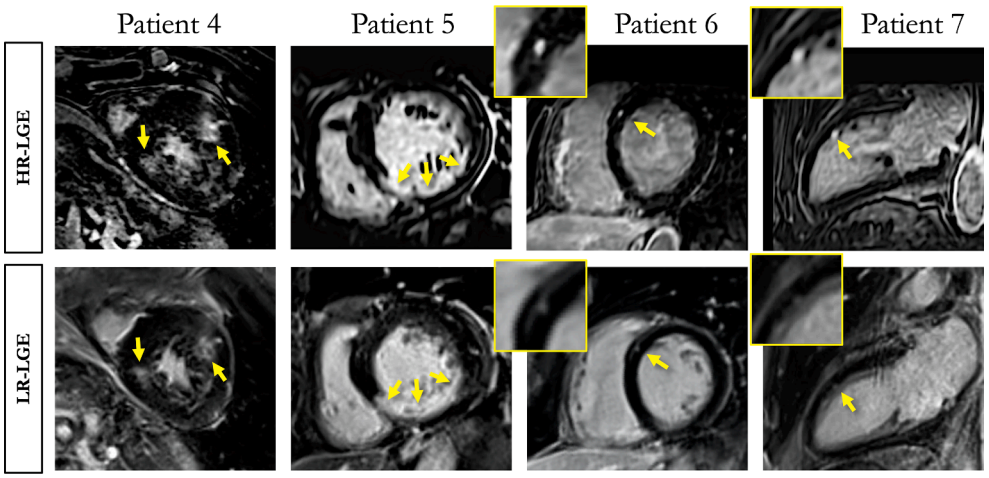

Fig. 4. Comparisons of reformatted free-breathing 3D HR-LGE and breath-held 3D LR-LGE in four patients (test cohort) presenting with various patterns of enhancement. Yellow arrows indicate LGE. *Patient 4*: 70-year-old man with hypertrophic cardiomyopathy associated with focal fibrosis. *Patient 5*: 62-year-old woman with inferior and inferoseptal myocardial infarction. *Patient 6*: 45-year-old man with arrhythmogenic right ventricular dysplasia, showing focal septal LGE. *Patient 7*: 48-year-old male patient with focal sub-endocardial LGE consistent with micro-infarction in the left anterior descending artery territory.

The spectrum of myocardial injuries on LGE imaging is illustrated in Figs. 5 and 6. Overall, a definite diagnosis was obtained in 15/20 patients, including myocarditis in 9, multiple microinfarctions in 2, myocardial infarction in 2, takotsubo cardiomyopathy in 2. One additional patient showed signs of acute pericarditis on LGE and T2 imaging but with no signs of myocardial injury. The 4 remaining patients had normal findings on CMR, and no definite diagnosis could be retained. Edema was found on T2 imaging in 8/9 patients with a diagnosis of myocarditis, and in 2/2 patients with a diagnosis of microinfarction. In these 10 patients with edema, the median delay since the onset of symptoms was 28 [16 –33] days. The 2 patients diagnosed with takotsubo showed typical wall motion abnormalities on TTE in the acute phase, and negative T2, LGE and cine imaging on the CMR study performed 54 and 20 days after the onset of symptoms. The 4 patients with no definite diagnosis showed a troponin peak of 414 ± 660 ng/mL, normal TTE and ECG findings in the acute phase, and normal CMR results 40 ± 33 days after the onset of symptoms.

4. Discussion

In this study, we demonstrate the feasibility of an accelerated free-breathing high-resolution 3D whole-heart LGE technique for the detection of COVID-related myocardial injuries. The main findings of the present study are that undersampled free-breathing isotropic HR-LGE improves the detection of myocardial defects as compared to conventional breath-held LR-LGE, and that the method allows for detailed characterization of COVID-related myocardial injuries in acceptable scan times.

4.1. Accelerated HR-LGE imaging in the context of COVID

The present study shows that undersampled (x3.8) free-breathing high-resolution isotropic LGE in concert with patch-based reconstruction enables the identification of more injured myocardial segments and improves diagnostic confidence as compared to conventional breath-held LGE methods. This improved sensitivity was equally observed in patients with structural heart diseases and in COVID patients. This is consistent with prior studies applying free-breathing LGE methods to the context of MINOCA [9] or to the etiological diagnosis of patients with ventricular arrhythmias [23].

Several recent studies have introduced isotropic HR-LGE techniques and their potential clinical utility in patients with repaired tetralogy of Fallot (resolution 1.3 mm^3, acquisition time ~ 7 min, [24]) or myocardial infarction and referred for ventricular tachycardia ablation (resolution 1.4 mm^3, acquisition time ~ 16 min, [12,13,25,26]) or cardiac resynchronization therapy [27].

In the present work, we thought to implement an LGE method specifically suited to the detection of COVID-related myocardial injuries. Because prior reports have shown that cardiac involvement in COVID patients is usually asymptomatic [7] and most often missed on TTE [28], we have anticipated that efficient scan times would be mandatory to allow for the screening of quite large populations on CMR. In addition, prior CMR studies in COVID patients showed that myocardial injuries are most often of small size [8,29,30], justifying efforts to improve the spatial resolution of LGE imaging. Last, the free-breathing approach further alleviated the need for repeated breath holds in COVID patients with impaired respiratory function.

The undersampled free-breathing technique proposed here allows for LGE imaging with near-millimetric isotropic spatial resolution with an overall image quality that favourably compares to the conventional breath held LGE method. The choice of using patch-based low-rank reconstruction over other non-linear reconstruction tools such as compressed sensing [11,31] was motivated by the fact that HR-LGE images contain a rich amount of similar information on a patch scale which can be efficiently exploited though patch-based low-rank reconstruction and consequently lead to better image quality, as previously demonstrated [14,32]. The x3.8 acceleration factor allows for scan times consistently below 10 min for HR-LGE, resulting in a complete CMR protocol duration below 40 min, which is in our opinion compatible with most clinical workflows, and acceptable even in frail COVID patients.

4.2. Spectrum of HR-LGE findings in COVID-19 patients

This study is the first to report on the use of HR-LGE CMR to diagnose the underlying cause of myocardial injury after COVID-19 infection. HR-LGE CMR appears to be extremely useful in this indication, identifying a cause in the vast majority of patients. In contrast, echocardiography and 12-lead ECG are poorly sensitive and specific, and our results indicate that LR-LGE may also miss subtle defects. Although acute myocarditis is the most common diagnosis, ischemic injuries and takotsubo cardiomyopathy can also be observed. These diagnoses are consistent with prior reports [8]. Both ischemic and inflammatory injuries may be associated with sub-acute myocardial edema persisting after one month, which is also consistent with prior studies [33].

Future research should aim at clarifying the pathophysiological mechanisms leading to each pattern of COVID-19-related myocardial injury, as well as their prognostic and therapeutic implications. One rather alarming aspect lies in the observation that most of the studied patients do not present with cardiac-specific clinical symptoms. These findings outline the need for systematic troponin tests during the acute phase of COVID-19 infection, and for a broader use of HR-LGE CMR in patients with history of COVID-19 infection. Indeed, silent scars may be

Table 3
Patient characteristics in the acute phase of COVID-19 infection (N = 20).

Demographics		**Transthoracic echocardiography**	
Age, years	46 ± 24	Negative, N (%)	9 (45)
Male gender, N (%)	15 (75)	LV wall motion abnormalities, N (%)	3 (15)
Risk factors and history		LVEF impairment, N (%)	3 (15)
Obesity, N (%)	7 (35)	RV dilatation or dysfunction, N (%)	1 (5)
Mean body mass index, kg/m^2	25 ± 7	**12-lead electrocardiogram**	
Smoking, N (%)	5 (25)	Negative, N (%)	12 (60)
Hypertension, N (%)	7 (35)	Atrial fibrillation, N (%)	1 (5)
Diabetes, N (%)	2 (10)	Non-specific T wave changes, N (%)	5 (25)
Chronic heart disease, N (%)	2 (10)	Right bundle branch block, N (%)	2 (10)
Acute clinical presentation		Monomorphic PVCs, N (%)	2 (10)
Fever > 38 °C, N (%)	13 (65)	Antiviral, N (%)	9 (45)
Arthromyalgia, N (%)	9 (45)	Antibiotic, N (%)	13 (65)
Asthenia, N (%)	14 (70)	Corticosteroids, N (%)	6 (30)
Anosmia or ageusia, N (%)	7 (35)	Tocilizumab, N (%)	5 (25)
Chest pain, N (%)	7 (35)	Hydroxychloroquine, N (%)	7 (35)
Dyspnea, N (%)	10 (50)	Anticoagulation, N (%)	9 (45)
Coughing, N (%)	12 (60)	Mechanical ventilation, N (%)	5 (25)
Abdominal symptoms, N (%)	7 (35)	**Acute complications**	
Cephalalgia, N (%)	5 (25)	ARDS, N (%)	5 (25)
COVID-19 diagnosis*		Ventricular arrhythmia, N (%)	2 (10)
Chest CT suggestive of COVID-19, N (%)	11/13 (85)	Atrial arrhythmia, N (%)	2 (10)
Positive COVID-19 PCR test, N (%)	16 (80)	Pulmonary embolism, N (%)	3 (15)
Positive COVID-19 serology, N (%)	4 (20)	Liver injury, N (%)	2 (10)
Laboratory findings		Renal failure, N (%)	3 (15)
C-reactive protein, mg/L, median [IQR]	88 [59–175]		
Fibrinogen, g/L, mean ± SD	7.1 ± 2.3		
NT-proBNP, pg/mL, median [IQR]	422 [41–879]		
Troponin I, ng/mL, median [IQR]	305 [83–1134]		

* Results are expressed as a fraction of the total number of subjects undergoing each diagnostic test. ARDS: acute respiratory distress syndrome; CT: computed tomography; EF: ejection fraction; IQR: interquartile range Q1-Q3; LV: left ventricle; PVCs: premature ventricular complexes; RV: right ventricle; SD: standard deviation.

highly prevalent and largely under detected in the infected population, particularly considering that a vast majority of patients is managed outside of hospitals and without laboratory tests to detect potential myocardial injury. Silent myocardial scars are known to be associated with adverse outcomes, exposing to higher risks of ventricular arrhythmia and sudden cardiac death over the long term [34,35]. Thus, there is a critical and urgent need to assess the prevalence of silent scars in the population infected by COVID-19, in order to better appreciate the cardiac risk that the pandemic may weigh on the global population in the near future. In that prospect, the accelerated and high-resolution

Table 4
CMR findings in the COVID-19 cohort (N = 20).

Timing of the CMR study		**Tissue characterization***	
Delay from onset to CMR, days, median [IQR]	30 [15–58]	LV native T1, ms, mean ± SD	1028 ± 59
Clinical symptoms at the time of CMR		LV ECV, %, mean ± SD	24.6 ± 2.5
Fever > 38 °C, N (%)	1 (5)	LV T2, ms, mean ± SD	49 ± 4
Arthromyalgia, N (%)	2 (10)	Focal edema on T2 imaging, N (%)	10 (50)
Asthenia, N (%)	8 (40)	LGE positive, N (%)	13/20 (65)
Anosmia or ageusia, N (%)	1 (5)	Subendocardial LGE, N (%)	3/20 (15)
Chest pain, N (%)	4 (20)	Subepicardial or intramural LGE, N (%)	9/20 (45)
Dyspnea, N (%)	2 (10)	Transmural LGE, N (%)	1/20 (5)
Coughing, N (%)	3 (15)	LGE burden, N segments, median [IQR]	1 [0–2]
Abdominal symptoms, N (%)	2 (10)	RV LGE, N (%)	0/20 (0)
Cephalalgia, N (%)	0 (0)	Pericardial LGE, N (%)	1/20 (5)
Ventricular function		**Final diagnosis**	
LVEDVi, mL/m^2, mean ± SD	78 ± 19	Myocarditis, N (%)	9 (45)
LVEF, %, mean ± SD	56 ± 12	Multiple micro-infarction, N (%)	2 (10)
LV wall motion abnormality, N (%)	4 (20)	Myocardial infarction, N (%)	2 (10)
RVEDVi, mL/m^2, mean ± SD	80 ± 14	Takotsubo cardiomyopathy, N (%)	2 (10)
RVEF, %, mean ± SD	49 ± 9	Pericarditis, N (%)	1 (5)
RV wall motion abnormality, N (%)	0 (0)	Negative CMR, N (%)	4 (20)
Pericardial effusion, N (%)	1 (5)		

* In 2/20 patients LGE results are based on LR-LGE only because HR-LGE was not completed. Abbreviations: CMR, cardiac magnetic resonance; ECV, extracellular volume fraction; EDV, end-diastolic volume index; EF, ejection fraction; LGE, late gadolinium enhancement; LV, left ventricle; IQR, interquartile range Q1-Q3; RV, right ventricle; SD, standard deviation.

LGE technique proposed here may be key to optimize CMR sensitivity.

4.3. Study limitations

A limitation of the current study is the unpredictable scan time given by the diaphragmatic navigated technique, where only a fraction of the acquired data is accepted for reconstruction (42 ± 10 % in the present series). Future work should aim at integrating alternate methods to compensate for respiratory motion without impairing scan efficiency, such as image-based navigation [36] or self-navigation [37].

Unfortunately, there was no reference standard for the detection of LGE in this study due to the absence of systematic endomyocardial biopsies to obtain diagnostic confirmation. Endomyocardial biopsy is not part of the routine diagnostic workup in our research centre. Instead, breath-held LR-LGE was used for comparison as this is the reference technique used in our center for assessment of LGE.

One limitation of the study is that the order of the LR-LGE and HR-LGE acquisitions was not randomized, as we could not deviate from our standard clinical protocol in these patients. Even though the relationship between blood and normal myocardium remains in a dynamic equilibrium up to 25 min after contrast injection [38], one may expect an improved scar-to-blood contrast on HR-LGE images as this sequence was always performed after LR-LGE and 15–20 min post injection.

Moreover, the prolonged acquisition for HR-LGE can be accompanied by a linear decrease in contrast agent concentration in the blood which could hamper image contrast. Mechanisms based on a gradually increasing TI could be easily integrated into our framework to take into account this effect [39].

Finally, qualitative comparisons with fully sampled HR-LGE dataset

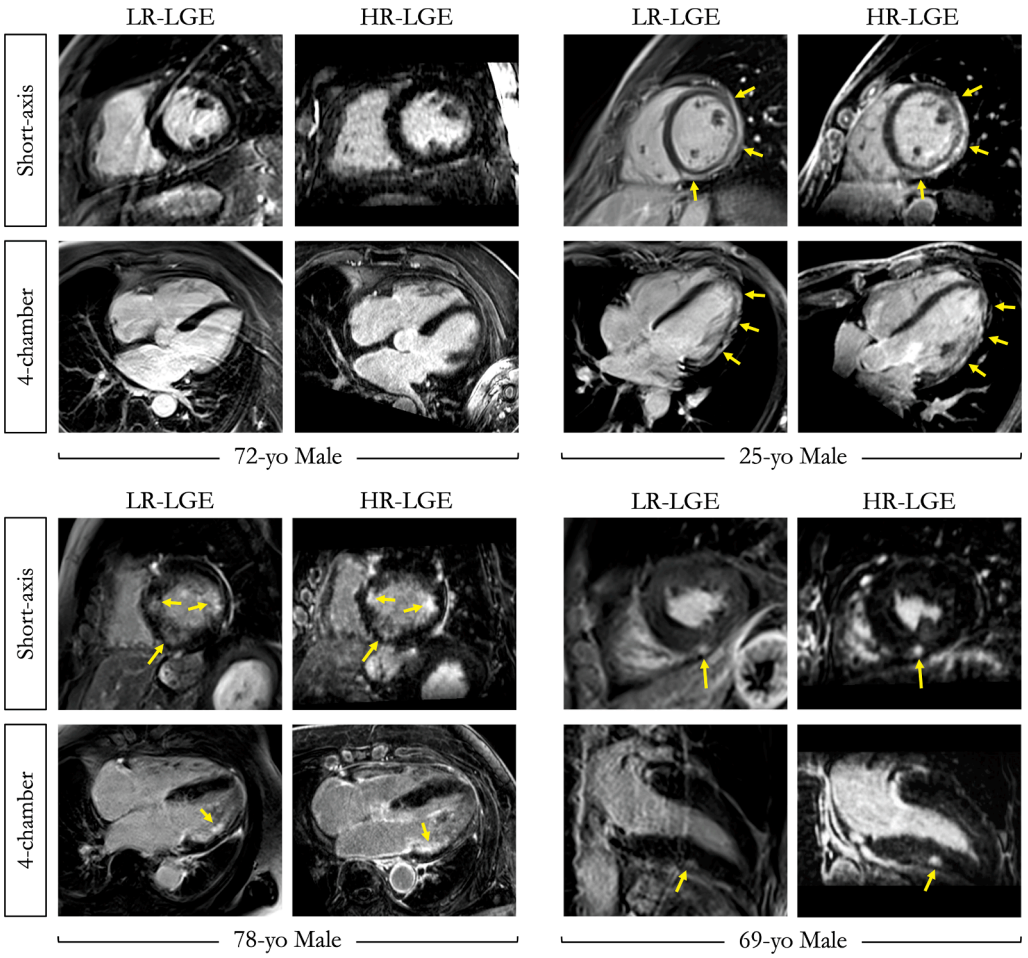

Fig. 5. Image quality comparisons between conventional breath-held low-resolution LGE (LR-LGE) and the proposed free-breathing high-resolution LGE (HR-LGE, reformatted images) sequence in four patients with laboratory-confirmed COVID-19 infection associated with troponin rise. The final diagnoses were negative CMR (top left), myocardial infarction (bottom left), acute myocarditis (top right and bottom right). Yellow arrows indicate sites of LGE.

could not be performed in vivo since it would have come with the caveat of unpractically long (near half an hour) acquisition times and accordingly unfair comparisons due to gadolinium washout and accumulation of motion artefacts. However, phantom experiments supported the use of acceleration factors up to x3.8 to spatially resolve fine structures and recover native image sharpness.

5. Conclusions

Undersampled free-breathing isotropic HR-LGE can detect additional areas of late enhancement as compared to conventional breath-held LR-LGE. In patients with history of COVID-19 infection associated with troponin rise, the method allows for detailed characterization of myocardial injuries in acceptable scan times and without the need for repeated breath holds. Although acute myocarditis is the most common diagnosis, ischemic injuries and takotsubo cardiomyopathy can also be observed. Additional CMR studies are needed to assess the prevalence of occult myocardial scars in the vast majority of infected subjects in whom cardiac troponin was not tested.

Ethics approval and consent to participate

This study was approved by the Biomedical Research Ethics Committee. All patients provided informed consent for participation in this study.

Research Data for this Article

The imaging protocol of the proposed 3D whole-heart HR-LGE sequence as well as the reconstruction framework are available from the corresponding author on reasonable request.

CRediT authorship contribution statement

Aurélien Bustin: Conceptualization, Methodology, Software, Validation, Formal analysis, Data curation, Writing – review & editing. **Soumaya Sridi:** Conceptualization, Methodology, Software, Validation, Formal analysis, Data curation, Writing – review & editing. **Pierre Gravinay:** Conceptualization, Data curation, Writing – original draft. **Benoit Legghe:** . **Philippe Gosse:** Conceptualization, Data curation, Writing – original draft. **Alexandre Ouattara:** Conceptualization, Data curation, Writing – original draft. **Hadrien Rozé:** Conceptualization, Data curation, Writing – original draft. **Pierre Coste:** Conceptualization, Data curation, Writing – original draft. **Edouard Gerbaud:** Conceptualization, Data curation, Writing – original draft. **Arnaud Desclaux:** Conceptualization, Data curation, Writing – original draft. **Alexandre Boyer:** Conceptualization, Data curation, Writing – original draft. **Renaud Prevel:** Conceptualization, Data curation, Writing – original draft. **Didier Gruson:** Conceptualization, Data curation, Writing – original draft. **Fabrice Bonnet:** Conceptualization, Data curation, Writing – original draft. **Nahema Issa:** Conceptualization, Data curation, Writing – original draft. **Michel Montaudon:** Conceptualization, Data curation, Writing – original draft. **Francois Laurent:** Conceptualization, Data curation, Writing – original draft. **Matthias Stuber:** Conceptualization, Data curation, Writing – original draft. **Fabrice Camou:** Conceptualization, Data curation, Writing – original draft. **Hubert Cochet:** Conceptualization, Methodology, Software, Validation, Formal analysis, Data curation, Writing – review & editing.

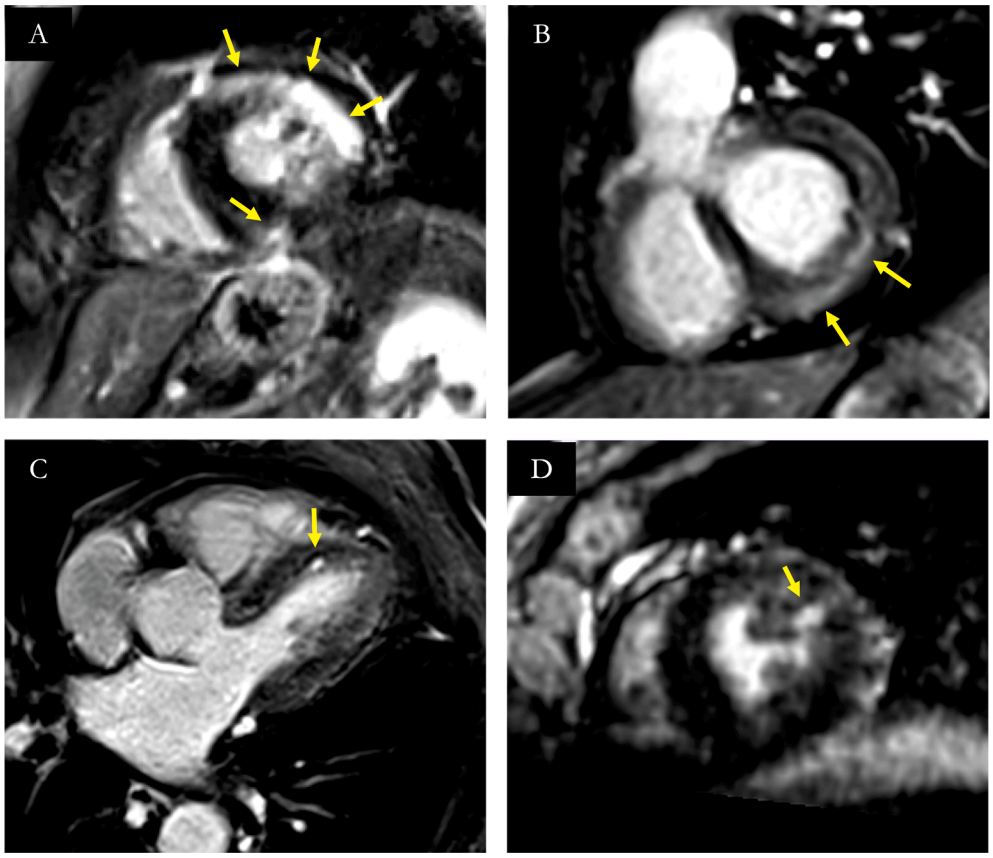

Fig. 6. Spectrum of myocardial injuries on reformatted free-breathing high-resolution LGE after COVID-19 infection. Yellow arrows indicate areas with LGE. A: intramural and sub-epicardial LGE on the anterio-lateral and infero-septal segments, consistent with myocarditis. B: subepicardial LGE on infero-basal and infero-latero-basal segments, consistent with myocarditis. C: focal sub-endocardial LGE on antero-septal segment consistent with micro-infarction. D: focal subendocardial LGE on antero-lateral segment consistent with micro-infarction.

Declaration of Competing Interest

The authors declare that they have no known competing financial interests or personal relationships that could have appeared to influence the work reported in this paper.

Acknowledgements

This research was supported by fundings from the French National Research Agency under grant agreements Equipex MUSIC ANR-11-EQPX-0030 and Programme d'Investissements d'Avenir ANR-10-IAHU04-LIRYC, and from the European Council under grant agreement ERC n715093. A.B. acknowledges a Lefoulon-Delalande Foundation fellowship administered by the Institute of France.

References

[1] M. Nishiga, D.W. Wang, Y. Han, D.B. Lewis, J.C. Wu, COVID-19 and cardiovascular disease: from basic mechanisms to clinical perspectives, Nat. Rev. Cardiol. 17 (2020) 543–558, https://doi.org/10.1038/s41569-020-0413-9.

[2] S. Shi, M. Qin, B. Shen, Y. Cai, T. Liu, F. Yang, W. Gong, X. Liu, J. Liang, Q. Zhao, H. Huang, B. Yang, C. Huang, Association of Cardiac Injury with Mortality in Hospitalized Patients with COVID-19 in Wuhan, China, JAMA Cardiol. 5 (2020) 802–810, https://doi.org/10.1001/jamacardio.2020.0950.

[3] T. Guo, Y. Fan, M. Chen, X. Wu, L. Zhang, T. He, H. Wang, J. Wan, X. Wang, Z. Lu, Cardiovascular Implications of Fatal Outcomes of Patients with Coronavirus Disease 2019 (COVID-19), JAMA Cardiol. 5 (2020) 811–818. https://doi.org/10.1001/jamacardio.2020.1017.

[4] A. Lala, K.W. Johnson, J.L. Januzzi, A.J. Russak, I. Paranjpe, F. Richter, S. Zhao, S. Somani, T. Van Vleck, A. Vaid, F. Chaudhry, J.K. De Freitas, Z.A. Fayad, S. P. Pinney, M. Levin, A. Charney, E. Bagiella, J. Narula, B.S. Glicksberg, G. Nadkarni, D.M. Mancini, V. Fuster, Prevalence and Impact of Myocardial Injury in Patients Hospitalized With COVID-19 Infection, J. Am. Coll. Cardiol. 76 (2020) 533–546, https://doi.org/10.1016/j.jacc.2020.06.007.

[5] A.R. Chapman, A. Bularga, N.L. Mills, High-Sensitivity Cardiac Troponin Can Be an Ally in the Fight against COVID-19, Circulation 141 (2020) 1733–1735, https://doi.org/10.1161/CIRCULATIONAHA.120.047008.

[6] S. Agewall, J.F. Beltrame, H.R. Reynolds, A. Niessner, G. Rosano, A.L.P. Caforio, R. De Caterina, M. Zimarino, M. Roffi, K. Kjeldsen, D. Atar, J.C. Kaski, U. Sechtem, P. Tornvall, ESC working group position paper on myocardial infarction with non-obstructive coronary arteries, Eur. Heart J. 38 (2017) 143–153, https://doi.org/10.1093/eurheartj/ehw149.

[7] V.O. Puntmann, M.L. Carerj, I. Wieters, M. Fahim, C. Arendt, J. Hoffmann, A. Shchendrygina, F. Escher, M. Vasa-Nicotera, A.M. Zeiher, M. Vehreschild, E. Nagel, Outcomes of Cardiovascular Magnetic Resonance Imaging in Patients Recently Recovered from Coronavirus Disease 2019 (COVID-19), JAMA Cardiol. 5 (2020) 1265–1273. https://doi.org/10.1001/jamacardio.2020.3557.

[8] T. Kotecha, D.S. Knight, Y. Razvi, K. Kumar, K. Vimalesvaran, G. Thornton, R. Patel, L. Chacko, J.T. Brown, C. Coyle, D. Leith, A. Shetye, B. Ariff, R. Bell, G. Captur, M. Coleman, J. Goldring, D. Gopalan, M. Heightman, T. Hillman, L. Howard, M. Jacobs, P.S. Jeetley, P. Kanagaratnam, O.M. Kon, L.E. Lamb, C. H. Manisty, P. Mathurdas, J. Mayet, R. Negus, N. Patel, I. Pierce, G. Russell, A. Wolff, H. Xue, P. Kellman, J.C. Moon, T.A. Treibel, G.D. Cole, M. Fontana, Patterns of myocardial injury in recovered troponin-positive COVID-19 patients assessed by cardiovascular magnetic resonance, Eur. Heart J. (2021) 1–13, https://doi.org/10.1093/eurheartj/ehab075.

[9] P.F. Lintingre, H. Nivet, S. Clément-Guinaudeau, C. Camaioni, S. Sridi, O. Corneloup, E. Gerbaud, P. Coste, G. Dournes, V. Latrabe, F. Laurent, M. Montaudon, H. Cochet, High-Resolution Late Gadolinium Enhancement Magnetic Resonance for the Diagnosis of Myocardial Infarction With Nonobstructed Coronary Arteries, JACC Cardiovasc. Imaging. 13 (2020) 1135–1148, https://doi.org/10.1016/j.jcmg.2019.11.020.

[10] S. Toupin, T. Pezel, A. Bustin, H. Cochet, Whole-Heart High-Resolution Late Gadolinium Enhancement: Techniques and Clinical Applications, J. Magn. Reson. Imaging. (2021) 1–21, https://doi.org/10.1002/jmri.27732.

[11] L. Pennig, S. Lennartz, A. Wagner, M. Sokolowski, M. Gajzler, S. Ney, K. R. Laukamp, T. Persigehl, A.C. Bunck, D. Maintz, K. Weiss, C.P. Naehle, J. Doerner, Clinical application of free-breathing 3D whole heart late gadolinium enhancement cardiovascular magnetic resonance with high isotropic spatial resolution using Compressed SENSE, J. Cardiovasc. Magn. Reson. 22 (2020) 1–13, https://doi.org/10.1186/s12968-020-00673-5.

[12] J. Fernández-Armenta, A. Berruezo, D. Andreu, O. Camara, E. Silva, L. Serra, V. Barbarito, L. Carotenutto, R. Evertz, J.T. Ortiz-Pérez, T.M. De Caralt, R.J. Perea, M. Sitges, L. Mont, A. Frangi, J. Brugada, Three-dimensional architecture of scar and conducting channels based on high resolution ce-CMR: Insights for ventricular tachycardia ablation, Circ. Arrhythmia Electrophysiol. 6 (2013) 528–537, https://doi.org/10.1161/CIRCEP.113.000264.

[13] D. Andreu, J.T. Ortiz-Pérez, J. Fernández-Armenta, E. Guiu, J. Acosta, S. Prat-González, T.M. De Caralt, R.J. Perea, C. Garrido, L. Mont, J. Brugada, A. Berruezo, 3D delayed-enhanced magnetic resonance sequences improve conducting channel

delineation prior to ventricular tachycardia ablation, Europace. 17 (2015) 938–945, https://doi.org/10.1093/europace/euu310.
[14] A. Bustin, G. Ginami, G. Cruz, T. Correia, T.F. Ismail, I. Rashid, R. Neji, R. M. Botnar, C. Prieto, Five-minute whole-heart coronary MRA with sub-millimeter isotropic resolution, 100% respiratory scan efficiency, and 3D-PROST reconstruction, Magn. Reson. Med. 81 (2019) 102–115, https://doi.org/10.1002/mrm.27354.
[15] J.Y. Cheng, T. Zhang, N. Ruangwattanapaisarn, M.T. Alley, M. Uecker, J.M. Pauly, M. Lustig, S.S. Vasanawala, Free-breathing pediatric MRI with nonrigid motion correction and acceleration, J. Magn. Reson. Imaging. 42 (2015) 407–420, https://doi.org/10.1002/jmri.24785.
[16] M. Lustig, D. Donoho, J. Santos, J. Pauly, Compressed Sensing MRI, IEEE Signal Process. Mag. 25 (2008) 1–18, https://doi.org/10.1109/MSP.2007.914728.
[17] A. Bustin, D. Voilliot, A. Menini, J. Felblinger, C. De Chillou, D. Burschka, L. Bonnemains, F. Odille, Isotropic Reconstruction of MR Images Using 3D Patch-Based Self-Similarity Learning, IEEE Trans. Med. Imaging. 37 (2018) 1932–1942, https://doi.org/10.1109/TMI.2018.2807451.
[18] P. Rajiah, M.Y. Desai, D. Kwon, S.D. Flamm, MR imaging of myocardial infarction, Radiographics. 33 (2013) 1383–1412, https://doi.org/10.1148/rg.335125722.
[19] M.G. Friedrich, U. Sechtem, J. Schulz-Menger, G. Holmvang, P. Alakija, L. T. Cooper, J.A. White, H. Abdel-Aty, M. Gutberlet, S. Prasad, A. Aletras, J.P. Laissy, I. Paterson, N.G. Filipchuk, A. Kumar, M. Pauschinger, P. Liu, Cardiovascular Magnetic Resonance in Myocarditis: A JACC White Paper, J. Am. Coll. Cardiol. 53 (2009) 1475–1487, https://doi.org/10.1016/j.jacc.2009.02.007.
[20] F.I. Marcus, W.J. McKenna, D. Sherrill, C. Basso, B. Bauce, D.A. Bluemke, H. Calkins, D. Corrado, M.G.P.J. Cox, J.P. Daubert, G. Fontaine, K. Gear, R. Hauer, A. Nava, M.H. Picard, N. Protonotarios, J.E. Saffitz, D.M.Y. Sanborn, J.S. Steinberg, H. Tandri, G. Thiene, J.A. Towbin, A. Tsatsopoulou, T. Wichter, W. Zareba, Diagnosis of arrhythmogenic right ventricular cardiomyopathy/dysplasia, Eur. Heart J. 31 (2010) 806–814, https://doi.org/10.1093/eurheartj/ehq025.
[21] W.G. Hundley, D.A. Bluemke, J.P. Finn, S.D. Flamm, M.A. Fogel, M.G. Friedrich, V. B. Ho, M. Jerosch-Herold, C.M. Kramer, W.J. Manning, M. Patel, G.M. Pohost, A.E. Stillman, R.D. White, P.K. Woodard, R.A. Harrington, J.L. Anderson, E.R. Bates, C. R. Bridges, M.J. Eisenberg, V.A. Ferrari, C.L. Grines, M.A. Hlatky, A.K. Jacobs, S. Kaul, R.C. Lichtenberg, J.R. Lindner, D.J. Moliterno, D. Mukherjee, R.S. Rosenson, R.S. Schofield, S.J. Shubrooks, J.H. Stein, C.M. Tracy, H.H. Weitz, D.J. Wesley, ACCF/ACR/AHA/NASCI/SCMR 2010 expert consensus document on cardiovascular magnetic resonance: A report of the american college of cardiology foundation task force on expert consensus documents, Circulation. 121 (2010) 2462–2508. https://doi.org/10.1161/CIR.0b013e3181d44a8f.
[22] L.Y. Hsu, A. Natanzon, P. Kellman, G.A. Hirsch, A.H. Aletras, A.E. Arai, Quantitative myocardial infarction on delayed enhancement MRI. Part I: Animal validation of an automated feature analysis and combined thresholding infarct sizing algorithm, J. Magn. Reson. Imaging. 23 (2006) 298–308, https://doi.org/10.1002/jmri.20496.
[23] A. Hennig, M. Salel, F. Sacher, C. Camaioni, S. Sridi, A. Denis, M. Montaudon, F. Laurent, P. Jais, H. Cochet, High-resolution three-dimensional late gadolinium-enhanced cardiac magnetic resonance imaging to identify the underlying substrate of ventricular arrhythmia, Europace. 20 (2018) f179–f191, https://doi.org/10.1093/europace/eux278.
[24] J. Stirrat, M. Rajchl, L. Bergin, D.J. Patton, T. Peters, J.A. White, High-resolution 3-dimensional late gadolinium enhancement scar imaging in surgically corrected Tetralogy of Fallot: clinical feasibility of volumetric quantification and visualization, J. Cardiovasc. Magn. Reson. 16 (2014) 76, https://doi.org/10.1186/s12968-014-0076-y.
[25] J. Acosta, J. Fernández-Armenta, D. Penela, D. Andreu, R. Borras, F. Vassanelli, V. Korshunov, R.J. Perea, T.M. De Caralt, J.T. Ortiz, G. Fita, M. Sitges, J. Brugada, L. Mont, A. Berruezo, Infarct transmurality as a criterion for first-line endo-epicardial substrate-guided ventricular tachycardia ablation in ischemic cardiomyopathy, Hear. Rhythm. 13 (2016) 85–95, https://doi.org/10.1016/j.hrthm.2015.07.010.
[26] D. Andreu, D. Penela, J. Acosta, J. Fernández-Armenta, R.J. Perea, D. Soto-Iglesias, T.M. de Caralt, J.T. Ortiz-Perez, S. Prat-González, R. Borràs, E. Guasch, J. M. Tolosana, L. Mont, A. Berruezo, Cardiac magnetic resonance–aided scar dechanneling: Influence on acute and long-term outcomes, Hear. Rhythm. 14 (2017) 1121–1128, https://doi.org/10.1016/j.hrthm.2017.05.018.
[27] J. Acosta, J. Fernández-Armenta, R. Borràs, I. Anguera, F. Bisbal, J. Martí-Almor, J. M. Tolosana, D. Penela, D. Andreu, D. Soto-Iglesias, R. Evertz, M. Matiello, C. Alonso, R. Villuendas, T.M. de Caralt, R.J. Perea, J.T. Ortiz, X. Bosch, L. Serra, X. Planes, A. Greiser, O. Ekinci, L. Lasalvia, L. Mont, A. Berruezo, Scar Characterization to Predict Life-Threatening Arrhythmic Events and Sudden Cardiac Death in Patients With Cardiac Resynchronization Therapy: The GAUDI-CRT Study, JACC Cardiovasc. Imaging. 11 (2018) 561–572, https://doi.org/10.1016/j.jcmg.2017.04.021.
[28] D.E. Clark, A. Parikh, J.M. Dendy, A.B. Diamond, K. George-Durrett, F.A. Fish, W. Fitch, S.G. Hughes, J.H. Soslow, COVID-19 myocardial pathology evaluated through screening cardiac magnetic resonance (compete CMR), MedRxiv. (2020), https://doi.org/10.1101/2020.08.31.20185140.
[29] L. Huang, P. Zhao, D. Tang, T. Zhu, R. Han, C. Zhan, W. Liu, H. Zeng, Q. Tao, L. Xia, Cardiac Involvement in Patients Recovered From COVID-2019 Identified Using Magnetic Resonance Imaging, JACC Cardiovasc. Imaging. 13 (2020) 2330–2339, https://doi.org/10.1016/j.jcmg.2020.05.004.
[30] H. Wang, R. Li, Z. Zhou, H. Jiang, Z. Yan, X. Tao, H. Li, L. Xu, Cardiac involvement in COVID-19 patients: mid-term follow up by cardiovascular magnetic resonance, J. Cardiovasc. Magn. Reson. 23 (2021), https://doi.org/10.1186/s12968-021-00710-x.
[31] G. Adluru, L. Chen, S.E. Kim, N. Burgon, E.G. Kholmovski, N.F. Marrouche, E.V. R. Dibella, Three-dimensional late gadolinium enhancement imaging of the left atrium with a hybrid radial acquisition and compressed sensing, J. Magn. Reson. Imaging. 34 (2011) 1465–1471, https://doi.org/10.1002/jmri.22808.
[32] T.A. Basha, M. Akçakaya, C. Liew, C.W. Tsao, F.N. Delling, G. Addae, L. Ngo, W. J. Manning, R. Nezafat, Clinical performance of high-resolution late gadolinium enhancement imaging with compressed sensing, J. Magn. Reson. Imaging. 46 (2017) 1829–1838, https://doi.org/10.1002/jmri.25695.
[33] M.Y. Ng, V.M. Ferreira, S.T. Leung, J.C. Yin Lee, A. Ho-Tung Fong, R.W. To Liu, J. W. Man Chan, A.K.L. Wu, K.C. Lung, A.M. Crean, I. Fan-Ngai Hung, C.W. Siu, Patients Recovered From COVID-19 Show Ongoing Subclinical Myocarditis as Revealed by Cardiac Magnetic Resonance Imaging, JACC, Cardiovasc. Imaging. (2020), https://doi.org/10.1016/j.jcmg.2020.08.012.
[34] E.B. Schelbert, J.J. Cao, S. Sigurdsson, T. Aspelund, P. Kellman, A.H. Aletras, C. K. Dyke, G. Thorgeirsson, G. Eiriksdottir, L.J. Launer, V. Gudnason, T.B. Harris, A. E. Arai, Prevalence and prognosis of unrecognized myocardial infarction determined by cardiac magnetic resonance in older adults, JAMA - J. Am. Med. Assoc. 308 (2012) 890–897, https://doi.org/10.1001/2012.jama.11089.
[35] Y.B. Pride, B.J. Piccirillo, C.M. Gibson, Prevalence, consequences, and implications for clinical trials of unrecognized myocardial infarction, Am. J. Cardiol. 111 (2013) 914–918, https://doi.org/10.1016/j.amjcard.2012.11.042.
[36] C. Munoz, A. Bustin, R. Neji, K.P. Kunze, C. Forman, M. Schmidt, R. Hajhosseiny, P. G. Masci, M. Zeilinger, W. Wuest, R.M. Botnar, C. Prieto, Motion-corrected 3D whole-heart water-fat high-resolution late gadolinium enhancement cardiovascular magnetic resonance imaging, J. Cardiovasc. Magn. Reson. 22 (2020) 1–13, https://doi.org/10.1186/s12968-020-00649-5.
[37] T. Rutz, D. Piccini, S. Coppo, J. Chaptinel, G. Ginami, G. Vincenti, M. Stuber, J. Schwitter, Improved border sharpness of post-infarct scar by a novel self-navigated free-breathing high-resolution 3D whole-heart inversion recovery magnetic resonance approach, Int. J. Cardiovasc. Imaging. 32 (2016) 1735–1744, https://doi.org/10.1007/s10554-016-0963-4.
[38] M. Ugander, A.J. Oki, L.-Y. Hsu, P. Kellman, A. Greiser, A.H. Aletras, C.T. Sibley, M.Y. Chen, W.P. Bandettini, A.E. Arai, Extracellular volume imaging by magnetic resonance imaging provides insights into overt and sub-clinical myocardial pathology, Eur. Heart J. 33 (2012) 1268–1278, https://doi.org/10.1093/eurheartj/ehr481.
[39] R.J. Holtackers, S. Gommers, C.M. Van De Heyning, C. Mihl, J. Smink, D. M. Higgins, J.E. Wildberger, R.M.A. ter Bekke, Steadily increasing inversion time improves blood suppression for free-breathing 3D late gadolinium enhancement MRI with optimized dark-blood contrast, Invest. Radiol. 56 (2021) 335–340, https://doi.org/10.1097/rli.0000000000000747.